Journal Pre-proof

Small molecule inhibitor of TAK1 ameliorates rat cartilaginous endplate degeneration induced by oxidative stress *in vitro* and *in vivo*

Pan Tang, Wen-Xiang Chen, Hong-Liang Gao, Jia-Yong Dai, Yu Gu, Zi-Ang Xie, Xiong-Feng Li, Shun-Wu Fan, Xue-Sheng Jiang, Qian Lu, Zhi-Jun Hu

PII: S0891-5849(19)31738-1

DOI: https://doi.org/10.1016/j.freeradbiomed.2020.01.002

Reference: FRB 14555

To appear in: *Free Radical Biology and Medicine*

Received Date: 15 October 2019

Revised Date: 1 January 2020

Accepted Date: 1 January 2020

Please cite this article as: P. Tang, W.-X. Chen, H.-L. Gao, J.-Y. Dai, Y. Gu, Z.-A. Xie, X.-F. Li, S.-W. Fan, X.-S. Jiang, Q. Lu, Z.-J. Hu, Small molecule inhibitor of TAK1 ameliorates rat cartilaginous endplate degeneration induced by oxidative stress *in vitro* and *in vivo*, *Free Radical Biology and Medicine* (2020), doi: https://doi.org/10.1016/j.freeradbiomed.2020.01.002.

Graphical Abstract

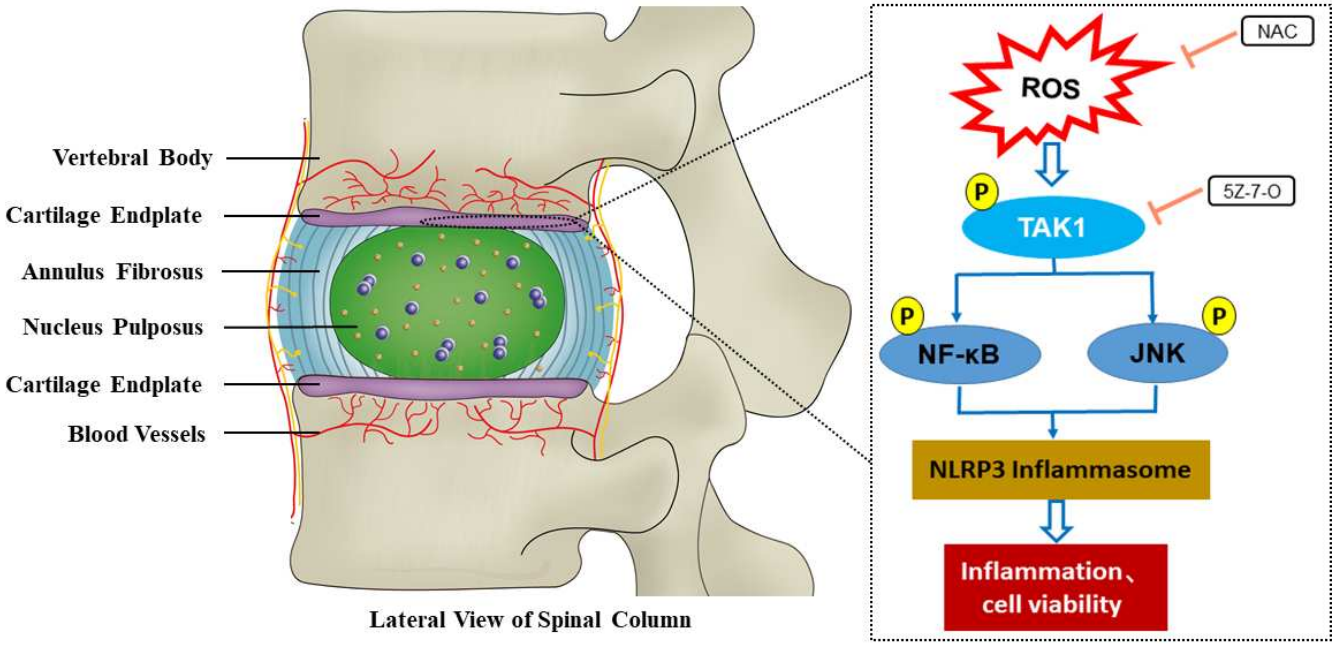

Small molecule inhibitor of TAK1 ameliorates rat cartilaginous endplate degeneration induced by oxidative stress *in vitro* and *in vivo.*

Pan Tang [a, c*], Wen-Xiang Chen [a*], Hong-Liang Gao [a*], Jia-Yong Dai [b, c], Yu Gu [b, c], Zi-Ang Xie [b, c], Xiong-Feng Li [a], Shun-Wu Fan [b, c], Xue-Sheng Jiang [a, c], Qian Lu [a], Zhi-Jun Hu [b, c]

[a] Department of Orthopaedic Surgery, Huzhou Central Hospital, Affiliated Central Hospital HuZhou University, #198 Hongqi Road, Huzhou 313003, China

[b] Department of Orthopaedic Surgery, Sir Run Run Shaw Hospital, Zhejiang University School of Medicine, China

[c] Key Laboratory of Musculoskeletal System Degeneration and Regeneration Translational Research of Zhejiang Province, Hangzhou 310016, China.

* These authors are contributed equally to this work.

Email:

Pan Tang, tangpan2012@qq.com

Wen-Xiang Chen, m15251827979@163.com

Hong-Liang Gao, gaoliang8877@163.com

Jia-Yong Dai, daijy1992@163.com

Zi-Ang Xie, xie_ziang@163.com

Yu Gu, qqqguyu@126.com

Xiong-Feng Li, 1107809566@qq.com

Xue-Sheng Jiang, 1203030957@qq.com

Shun-Wu Fan, srrshspine@gmail.com

Qian Lu, luqian19820207@163.com

Address correspondence and reprint requests to

Zhi-Jun Hu, PHD, Department of Orthopaedic Surgery, Sir Run Run Shaw Hospital, Zhejiang University School of Medicine, #3 East Qingchun Road, Hangzhou 310016,

China

E-mail: hzjspine@zju.edu.cn

Acknowledgments

The study was sponsored by National Natural Science Fund of China (81672150), Zhejiang medical and health science and technology project (2018KY117, 2019ZD041), New talent in medical field of Zhejiang Province, the fundamental research funds for the central universities (2019QNA7027), and Huzhou science and technology bureau project (2019GY04).

Introduction

Intervertebral disc degeneration (IVDD), a major cause of lower back pain (LBP), is the most common and disabling clinical problem in orthopedics. Further, it is considered a significant socioeconomic burden worldwide[1–3]. Intervertebral discs (IVDs) are avascular organs and each consists of a nucleus pulposus (NP), an annulus fibrosus (AF), and cartilage endplates (CEPs). The IVD is essentially the largest avascular structure in the human body[4]. Except for minor blood supply to the outer layers of the AF, nutrients supply to the disc and waste products carry away from the disc rely mainly on convective transport through the CEPs[5,6]. Therefore, endplate degeneration is closely associated with IVDD and can initiate or accelerate this condition by impeding nutrient transport to the disc[7,8]. Accordingly, studies on the mechanisms underlying CEP degeneration will be integral to develop effective therapeutic protocols for IVDD.

The lesions of degenerative CEPs were first observed by magnetic resonance imaging (MRI) by de Roos et al., and termed Modic changes, after M.T. Modic[9,10]. There are three different types of Modic changes[10]. Modic type 1 changes are hypointense on T1-weighted images and hyperintense on T2-weighted images, and indicate inflammation and edema in the lesions from histological perspective. Modic type 2 changes are hyperintense on T1-weighted images and isointense or hyperintense on T2-weighted images, and represent fatty replacement of the formerly red bone marrow as confirmed by histology. Modic type 3 changes are hypointense on T1- and T2-weighted images and reflect subchondral bone sclerosis. However, the exact molecular and mechanical mechanism underlying endplate degeneration remains poorly understood. An examination of oxidative stress markers indicated that oxidative stress, promoted by the overproduction of reactive oxygen species (ROS), might be involved in IVDD[11–13]. Suzuki et al. demonstrated that oxidative stress contributes to the progression of IVDD and exerts a catabolic effect on AF cells[14]. Moreover, two recent studies confirmed that oxidative stress is involved in pathologic CEP degeneration by decreasing autophagy and inducing apoptosis in CEP

chondrocytes[15], which causes CEP lesions[16]. It is known that oxidative stress is closely related to inflammation[17,18]. Furthermore, activation of the inflammasome, especially NACHT, LRR, and PYD domains-containing protein 3 (NLRP3), is reportedly induced by the overproduction of ROS[19–21]. In a previous study, we demonstrated activation of the NLRP3 – caspase-1 – interleukin-1β (IL-1β) axis in human degenerative lumbar CEP tissue[22]. Specifically, the NLRP3 inflammasome can trigger the proteolytic cleavage of pro-caspase-1 into biologically active caspase-1, which then converts the dormant cytokine precursor pro-IL-1β into mature and biologically active IL-1β[23]. As a potent pro-inflammatory mediator, mature IL-1β participates in many reactions. During IVDD, downstream IL-1β promotes the expression of disintegrin like and metalloproteinase thrombospondin type I motif5 (ADAMTS) and matrix metalloproteinases (MMPs), which can degrade the extracellular matrix proteins of CEPs[24,25].

Transforming growth factor β activated kinase 1 (TAK1) is closely related to a variety of pathophysiological processes through controlling nuclear factor-kB (NF-kB) and mitogen-activated protein kinase (MAPK) pathways[26]. As the upstream regulator of the NF-kB pathway, a number of studies have indicated that TAK1 is tightly related to spinal diseases and cartilage homeostasis[27,28]. What`s more, a recent study showed that inhibition of TAK1 prevents inflammation-related cartilage degradation in osteoarthritis[29].

However, activation of the NLRP3 signaling pathway in CEPs in response to oxidative stress induced by excessive ROS has not yet been studied. And the specific role TAK1 plays in IVDD pathogenesis still remains to be clarified. Therefore, the present study investigated the role of excessive ROS in the pathogenesis of degenerative CEPs and determined if inhibiting the downstream ROS signaling pathway could be a therapeutic target for this condition.

Materials and Methods

Human samples

Experimental protocols and the use of surgical samples were approved by the Ethics Committee of Sir Run Run Shaw Hospital, Medical College of Zhejiang University. Endplate tissues without Modic changes were collected from three male patients and one female patient, aged 21 – 36 years (mean, 25.96), with vertebral burst fractures as controls. Degenerative tissues were collected from five male and seven female patients, aged 34–77) years (mean, 57.6) with Modic changes undergoing spinal surgery. The cartilaginous endplate tissues were sectioned for use in different experiments immediately, as previously described[22,24] Briefly, we conducted histological analyses via hematoxylin and eosin, as well as safranin O, staining, detected changes in ROS levels, explored marker genes using RT-PCR, and analyzed the expression of NLRP3, pro-caspase-1, caspase-1, pro-IL-1β, IL-1β, transforming growth factor b-activated kinase-1 (TAK1), and β-actin (1:1000; Cell Signaling Technology, Boston, MA, USA) by western blotting. We also checked the expression of IL-1β using enzyme-linked immunosorbent assays ELISAs. Primers used are listed (Table 1).

ELISA

ELISA Kits (Thermo Fisher Scientific) were used to quantify IL-1β in the endplate homogenate or cell culture supernatants. Experiments were performed in duplicate according to the manufacturer's recommendations.

Cell culture

According to a previous study[30], rat endplate tissues were macroscopically dissected from the lumbar IVD of 4-week-old female Sprague Dawley (SD) rats and digested overnight using collagenase II (0.025 %) (Roche Diagnostics, Tokyo, Japan) at 37 °C. Endplate chondrocytes were then washed with Dulbecco's modified Eagle's medium (DMEM; Invitrogen, Carlsbad, CA, USA) containing 5 % heat-inactivated fetal bovine serum (FBS; JRH Biosciences, Lenexa, KS, USA) according to a previously described method. Isolated endplate chondrocytes were cultured in DMEM

supplemented with 10 % FBS, maintained in a humidified incubator containing 5 % CO_2 at 37 °C, and used within the first two passages for experiments that followed.

Oxidative stress and antioxidant treatments

To evaluate oxidation in the endplate, chondrocytes were treated with H_2O_2 (Wako, Tokyo, Japan) for 24 h. To study the effects of antioxidants or small molecular agents, N-acetyl cysteine (NAC, 1 g/l; Sigma, St. Louis, USA), MCC950 (Selleck, Houston, USA), and diacerein (Selleck, Houston, USA) were used to treat the chondrocytes for 30 min before administering H_2O_2.

Cell proliferation and viability analysis

Cell proliferation and viability under the following oxidative stress and antioxidant treatment regimens were estimated using a Cell Counting Kit-8 (Dojindo Laboratories, Kumamoto, Japan) according to the manufacturer's instructions. Chondrocytes were seeded in a 96-well plate (5000 cells/well) and cultured as described previously herein. Chondrocytes were then treated with different concentrations of H_2O_2 (0, 200, 400, 800, 1000, and 1200 μM), NAC (0, 1, 2, 4, 6, 8, and 10 mM), 5 μM MCC950, or 50 μM diacerein. Next, 10 μl of CCK-8 dye was added to each well, chondrocytes were incubated at 37 □ for 30 min, and optical density was estimated at 450 nm using a multi-mode microplate reader (Synergy2, BioTek, Winooski, VT).

Apoptosis analysis using flow cytometry

Apoptosis was assessed using an Annexin V-FITC-kit. Briefly, chondrocytes were seeded in 6-well plates (25×10^4 cells/well). Chondrocytes were washed twice with cold PBS (phosphate-buffered saline), resuspended in binding buffer with 5 μL Annexin V-FITC and 5 μL propidium iodide (PI), and then incubated for 15 min in the dark room. Samples were analyzed through flow cytometry within 1 h of staining.

Total superoxide dismutase (T-SOD) and MDA measurements

Analyses of T-SOD in the culture media of endplate chondrocytes were carried out according to the instructions of the manufacturers of the kits used (Nanjing Jiancheng

Bioengineering Institute, Nanjing, China). Briefly, 100 μL culture medium and reagents were mixed completely in tubes. Next, the mixture was heated for 60 min at 37°C. Following the addition of the developer into the samples at the room temperature for 10 min, the absorbance of supernatant was measured via spectrophotometry (Model UV-2401, Shimadzu Co.) at 550 nm. Determination of MDA was based on its reaction with thiobarbituric acid (TBA) to form red colored formazan. Briefly, 100 μl of plasma/standards were added to the tubes containing TBA dissolved in acetic acid. Samples were then boiled for 60 min at 95 °C, following which HCL and butanol were introduced into the mixture. After centrifugation at 3500 rpm for 10 min, the butanol phase was removed. The absorbance of the supernatant was measured via spectrophotometry at 532 nm.

Western blotting

The proteins in chondrocytes were extracted with radioimmune precipitation assay lysis buffer and boiled for 4 min in 5× loading buffer. Samples were separated on 10% sodium dodecyl sulfate polyacrylamide gel electrophoresis gels, and the proteins were transferred to polyvinylidene fluoride membranes (Bio-Rad) by electroblotting. The membranes were blocked using 5% (w/v) nonfat milk for 2 h at room temperature and incubated overnight at 4 °C with antibody against collagen II (Col II), matrix metalloproteinase-3 (MMP-13), a disintegrin like and metalloproteinase thrombospondin type I motif5 (ADAMTS-5), p-p65, p-65, p-JNK, JNK, p-TAK1, TAK1, NLRP3 (1:1000; Cell Signaling Technology, Boston, MA, USA), caspase-1, IL-1β, and β-actin (1:1000; Cell Signaling Technology), followed by incubation with secondary goat anti-rabbit horseradish peroxidase-conjugated antibody (CWBIO, Beijing, China) for 1 h. Proteins were assayed using ECL Western Blotting Detection Reagent (GE Healthcare, Uppsala, Sweden). Bands were quantified with Image J 1.49v software (Wayne Rasband, National Institutes of Health, Bethesda, MD, USA).

RT-PCR

Total RNA in chondrocytes was extracted using the RNeasy Mini Kit (Qiagen,

Valencia, CA, USA) according to the manufacturer's protocol. Next, the RNA was reverse-transcribed and amplified by PCR. Briefly, real-time RT-PCR was performed using the Thermal Cycler Dice Real-Time System and SYBR Premix Ex Taq (Takara Bio). Primers used are listed (Table 1). Mean Ct values of genes under investigation were normalized to β-actin and the results were quantified using the ddCt method.

Animal IVDD model and MRI evaluation

Thirty Sprague-Dawley rats (180 ± 10 g) purchased from the Shanghai Laboratory Animal Company (SLAC) were used as the animal model. We established the model by modifying the protocol of Han et al[31]. The tail discs were injected with 2 μl of various solutions including 0.1 M phosphate-buffered saline (PBS; sham group), 1000 μM H_2O_2, 2 mM NAC, or 2 mM 5Z-7-O. First, both subchondral bones of caudal level 6/7-8/9 were injected with H_2O_2. After 30 min, PBS, NAC, or 5Z-7-O was injected into the selected levels, respectively. The IVD at caudal level 5/6 remained undisturbed as the control group. Following the procedure, rats were raised in cages and given food and water for 4 weeks until euthanasia. Disc injection was performed using a 29-gauge insulin injector needle and the depth of the injection was determined by the resistance of tissue according to previous studies[32,33]. MRI was performed before the injection and at 4 weeks post-operatively as reported previously[34]. T2-weighted images were obtained, and the ratio of the high-intensity area to IVD was measured using Image J software 1.46.

Histological analysis

Rat endplate tissues were fixed in paraformaldehyde solution for 24 h, decalcified in 10% EDTA for 2 weeks, and then embedded in paraffin, sectioned, and stained with hematoxylin, eosin, and safranin-O. Cartilage area and endplate thickness were measured according to Zhou et al[35]. IVD was evaluated based on the scoring system (Table S1) described by Wang et al[36]. To evaluate IVDD by immunofluorescence, discs were incubated with primary antibodies for MMP13 and IL-1β. After staining, the number of positively stained cells and integrated optical densities in the discs were

analyzed according to our previous study[34].

Statistical analysis

Quantitative data are expressed as the mean ± SD. Differences among groups were analyzed by ANOVA, followed by post hoc Tukey HSD analysis to separate individual means. Statistical analyses were performed using SPSS 18.0 (IBM, Chicago, IL, USA). Statistical significance was set at $P < 0.05$.

Results

The NLRP3 inflammasome axis and TAK1 are activated in human CEP samples with Modic changes

Hematoxylin and eosin staining of human CEP tissue indicated that the extracellular matrix was fibrotic and sclerotic, with fewer chondrocytes in the Modic changes group, compared to that in the control group (Fig. 1A, B; $P < 0.05$). Additionally, safranin O staining showed a decrease in proteoglycan content in the Modic changes group (Fig. 1A). Further, the ROS levels were significantly increased in the endplates with Modic changes (Fig. 1C; $P < 0.05$). Gene expression results were consistent with histology, in that the extracellular matrix was degenerative in the Modic changes group. Phenotype marker genes encoding collagen II (Col II) and SOX-9 were downregulated in the Modic changes group compared to that in controls. In contrast, the expression of matrix metalloproteinase-3 (MMP-13) and ADAMTS-5 was upregulated in the Modic changes group (Fig. 1D; $P < 0.05$). We also analyzed expression of the NLRP3/caspase-1/IL-1β axis and TAK1 (Fig. 1E, F). The results were consistent with those of our previous study[22], indicating that the NLRP3 inflammasome axis is implicated in Modic changes and that TAK1 is upregulated in human CEP tissue with Modic changes.

NAC inhibits H_2O_2-induced rat endplate chondrocyte damage and oxidative stress

Annexin V-FITC staining and the viability of rat endplate chondrocytes treated for 24 h with different H_2O_2 concentrations was examined to clarify the pathophysiological

effect of intracellular ROS. Chondrocyte viability was suppressed significantly by H_2O_2 at the dose of 800 μM (Fig. 2A, B). However, no significant evidence of malondialdehyde (MDA), a lipid peroxidation marker, was found until a concentration of 1000 μM H_2O_2 was used (Fig. 2C; $P < 0.05$). Next, we investigated whether the administration of an antioxidant could attenuate H_2O_2-induced oxidative stress in rat endplate chondrocytes. First, it was confirmed that NAC levels lower than 2 mM did not affect the viability of endplate cells (Fig. 2D; $P > 0.05$). Endplate chondrocytes were then pretreated with NAC for 30 min, followed by H_2O_2 for 24 h. Endplate chondrocyte activity was significantly improved by NAC administration (Fig. 2E, F; $P < 0.001$). Further, administration of the NLRP3 inhibitor MCC950 and antagonist of IL-1β receptor diacerein also improved chondrocyte activity after H_2O_2 treatment (Fig. 2E, F). Next, we treated endplate chondrocytes with 1000 μM H_2O_2 for 24 h or pre-treated chondrocytes with 2 mM NAC for 30 min and oxidative stress was detected by measuring MDA levels (Fig. 2G) and T-SOD activity (Fig. 2H). The results indicated that H_2O_2 treatment significantly increased oxidative stress in endplate chondrocytes, and that pretreatment with NAC significantly decreased H_2O_2-mediated oxidative stress ($P < 0.05$). These results demonstrated that H_2O_2 might induce oxidative stress in endplate chondrocytes and that NAC could efficiently suppress this.

NAC inhibits H_2O_2-induced endplate chondrocyte extracellular matrix degradation

Next, we evaluated the effect of H_2O_2-induced oxidative stress on endplate chondrocyte extracellular matrix degradation via RT-PCR and western blotting. The mRNA expression of genes encoding catabolic enzymes such as MMP-13 and ADAMTS-5 was significantly increased when the chondrocytes were treated with H_2O_2, whereas that of Col II and SOX-9 was reduced (Fig. 3A; $P < 0.05$). However, pretreatment with NAC neutralized the catabolic effect of H_2O_2 significantly. Western blot and densitometric analyses showed that H_2O_2 treatment significantly enhanced the expression of catabolic enzymes and inhibited the expression of Col II and SOX-9 (Figs. 3B–F; $P < 0.05$). Further, catabolism induced by H_2O_2 was reduced by NAC

administration (Figs. 3B, D, and E; $P < 0.05$). Western blotting results, which confirmed the results of gene expression, showed the same tendency in H_2O_2-induced endplate chondrocytes. Considered together, these data indicated that oxidative stress induced by H_2O_2 has a catabolic effect on the extracellular matrix and that NAC alleviates the degeneration process in endplate chondrocytes.

NAC and 5Z-7-O inhibit the activation of signaling pathways and the NLRP3 inflammasome

Reportedly, ROS and activated p-p65 and p-JNK pathways generate crucial upstream signals, and thus blocking them might restrain activation of the NLRP3 inflammasome[37–39]. To determine the downstream signaling pathway through which H_2O_2 stimulates ROS in rat endplate chondrocytes, the phosphorylation of p65, JNK, and TAK1 was evaluated by western blotting. Results illustrated that stimulating chondrocytes with H_2O_2 activates the phosphorylation of p65, JNK, and TAK1 in a time-dependent manner (Fig. 4A–D). However, pretreating chondrocytes for 30 min with 5Z-7-oxozeaenol (5Z-7-O), a TAK1-specific small molecule inhibitor, inhibited the phosphorylation of p65 and TAK1 and expression of the NLRP3 inflammasome axis upon stimulation with H_2O_2 (Fig. 5). Moreover, pretreating chondrocytes with NAC for 30 min also inhibited the phosphorylation of p65 and TAK1, and significantly inhibited the activation of NLRP3, pro-caspase-1, caspase-1, pro-IL-1β, and IL-1β (Fig. 5). These results indicated that treatment with ROS scavengers, namely NAC and the TAK1-specific inhibitor 5Z-7-O, reduced the levels of activated TAK1 and p65. In addition, both downregulated expression of the NLRP3/caspase-1/IL-1β axis in H_2O_2-treated EP chondrocytes, confirming the chondroprotective effect of NAC and 5Z-7-O *in vitro*. In summary, these findings suggested that 5Z-7-O might inhibit the NLRP3 inflammasome pathway by targeting TAK1 (Fig. 6).

NAC and 5Z-7-O treatment ameliorate rat CEP degeneration in vivo

Finally, to explore the preventive effects of NAC and 5Z-7-O on CEP degeneration *in vivo*, these compounds were administered intra-disc to rats with H_2O_2-induced CEP

degeneration. Safranin O staining showed that the glycosaminoglycan content in the ECM and EP thickness were reduced in the PBS group (Fig. 7A, B) compared to those in the other groups. Further, the administration of NAC and 5Z-7-O upregulated glycosaminoglycan expression and restored endplate thickness contrast in the PBS group (Fig. 7A, B, D; $P < 0.05$). In addition, CEP chondrocytes were markedly reduced in the PBS group, and NAC and 5Z-7-O exerted a chondroprotective effect *in vivo* compared to those in the PBS group (Fig. 7B, C, F; $P < 0.05$). Hematoxylin and eosin staining of rat CEP tissue also showed that notochord cells were reduced in the ECM of the NP and that the outer AF was not arranged in well-ordered rows (Fig. 8A, B). Then, immunohistochemical staining of the IVD showed that the levels of MMP13 (Fig. 8C, F) and IL-1β (Fig. 8D, G) were high in the PBS group, indicating that the IVD was degenerative. However, after NAC and 5Z-7-O intervention, MMP13 staining intensity and IL-1β positive cells decreased compared to those in the PBS group. These results showed that NAC and 5Z-7-O inhibit enzymes that can degrade the matrix and can alleviate inflammation in the IVD. Further, histological scores, based on the disc degeneration assessment scoring system of Wang et al[36], showed that discs in the PBS group were graded as moderate, whereas those in the other groups were normal or mild (Fig 8E). Moreover, MRI signal intensity of IVDs treated with PBS decreased progressively at 4 weeks, whereas those treated with NAC and 5Z-7-O displayed a significantly higher signal intensity (Fig 8H, I). In summary, these results revealed that NAC and 5Z-7-O treatment ameliorate rat CEP degeneration *in vivo.*

Discussion

An H_2O_2-induced model of oxidative stress in the endplate was successfully established *in vitro* and *in vivo* in this study. Further, the ROS scavenger NAC alleviated cellular damage, abrogated catabolic effects, and restored the redox status and cell viability in endplate chondrocytes *in vitro* and *in vivo*. In addition, the small molecule inhibitor of TAK1 5Z-7-O reduced the expression of p-TAK1 and NLRP3

considerably and ameliorated rat CEP degeneration *in vivo*, indicating that the administration of 5Z-7-O might be a potential therapeutic target for CEP degeneration.

Previous research demonstrated that inflammation is a major mediator of the progression of Modic changes[40]. NLRP3 inflammasomes are also implicated in the degeneration of CEP[22]. The NLRP3 inflammasome and its final breakdown product, IL-1β, play an important role in the activation of catabolism in the extracellular matrix. Three factors are cited in the literature as facilitators of NLRP3 activation, namely ROS generation, ion fluxes, and phagosomal destabilization[19,21]. ROS have been suggested as common upstream mediators of NLRP3 activation. ROS also play a pivotal role in the progression of chondrocyte death and matrix degradation[41]. Based on this evidence, we proposed that ROS generation in the CEP might result in the inflammation response via NLRP3 inflammasome activation. In accordance with previous studies reporting that H_2O_2 can activate NLRP3 inflammasomes[42,43], we found that the administration of 1000 μM H_2O_2 for 24 h succeeded in inducing oxidative stress injury in chondrocytes, resulting in the upregulation of NLRP3. Results also indicated that H_2O_2 increased MDA content and decreased T-SOD activity, which exerted catabolic effects on the ECM of chondrocytes. Finally, pretreating degenerated, H_2O_2-stimulated chondrocytes with the antioxidant NAC significantly inhibited oxidative stress and NLRP3 activation *in vitro* and *in vivo*.

TAK1, a serine/threonine kinase, is a critical molecular component that regulates diverse functions related to cell fate determination[44]. Reportedly, TAK1 is considered an attractive therapeutic target for many cartilage-related diseases such as osteoarthritis and rheumatoid arthritis. TAK1 inhibition also prevents inflammation-related cartilage degeneration, suppresses downstream inflammatory mediators, and downregulates the expression of matrix metalloproteinases[45–48]. Furthermore, Onodera et al. demonstrated that H_2O_2 might activate ROS–TAK1–MAPK/NF-κB–COX2 signaling in synovial fibroblast cells and described an effective therapeutic strategy for chronic joint diseases[49]. Our results were consistent with

previous reports indicating that expression of the p-TAK1, p-p65, and NLRP3 axis is upregulated in endplate chondrocytes treated with H_2O_2, and that the ECM is degraded. Chondrocytes pretreated with NAC prior to H_2O_2 exposure exhibited increased cell viability and T-SOD activity, decreased MDA formation, maintained ECM production, inhibited p65 and TAK1 phosphorylation, and downregulated NLRP3, caspase-1, and IL-1β expression. A similar protective effect was observed with 5Z-7-O, prior to the administration of H_2O_2. However, phosphorylation of TAK1 was suppressed much more significantly with 5Z-7-O than with NAC. Moreover, the NLRP3 inflammasome was activated by ROS directly or via the activation of TAK1, which led to a downstream inflammation response in IVDs.

In the current study, we demonstrated that a ROS scavenger, namely NAC, can ameliorate endplate degeneration using an *in vitro* cell model and a rat model. Furthermore, we confirmed that the TAK1 inhibitor 5Z-7-O can alleviate endplate degeneration in the rat model. Considering these findings, recovering redox homeostasis of the endplate might be an effective measure to retard endplate degeneration, where 5Z-7-O exerts protective action against H_2O_2-induced endplate degeneration by inhibiting the TAK1–NLRP3 inflammasome pathway. Future studies could focus on the efficacy of 5Z-7-O treatment in larger preclinical trials involving animal endplate degeneration models, and subsequently, clinical trials might be performed to evaluate the effect of 5Z-7-O on IVD progression in patients.

There remain limitations in this study. First, many different chemical induction IVDD animal models were introduced in the previous studies, such as IL-1β, chymopapain, propionibacterium acnes and chondroitinase ABC et al. As far as we know, no related papers use the H_2O_2-induced animal model. However, H_2O_2 was widely used in cell models to explore the function and mechanism of oxidative stress in the degeneration of IVD. What`s more, researchers employed H_2O_2 to the *in vitro* model to detect the function of oxidative stress recently[50,51]. And our main purpose was to determine the molecular mechanism related to oxidative stress underlying endplate degeneration, so we used this model. Then, there is no denying that this model is neither good enough

in some aspects, such as effectiveness of treatment for the clinical situation, short treatment time, clinical relevance of occurrence and development of the IVDD. If this model can be confirmed by other researchers, it will be an ideal animal model to explore the oxidative stress in IVDD.

References

1. Adams MA, Roughley PJ. What is intervertebral disc degeneration, and what causes it? *SPINE* 2006;31:2151–61.
2. Vos T, Flaxman AD, Naghavi M, et al. Years lived with disability (YLDs) for 1160 sequelae of 289 diseases and injuries 1990-2010: A systematic analysis for the Global Burden of Disease Study 2010. *Lancet* 2012;380:2163–96.
3. Wai EK, Roffey DM, Bishop P, et al. Causal assessment of occupational lifting and low back pain: results of a systematic review. *Spine J* 2010;10:554–66.
4. Grunhagen T, Shirazi-Adl A, Fairbank JCT, et al. Intervertebral disk nutrition: a review of factors influencing concentrations of nutrients and metabolites. *Orthop Clin North Am* 2011;42:465–77, vii.
5. Colombier P, Clouet J, Hamel O, et al. The lumbar intervertebral disc: From embryonic development to degeneration. *Jt Bone Spine* 2014;81:125–9.
6. Moore RJ. The vertebral end-plate: what do we know? *Eur Spine J* 2000;9:92–6.
7. Gu W, Zhu Q, Gao X, et al. Simulation of the progression of intervertebral disc degeneration due to decreased nutritional supply. *SPINE* 2014;39:E1411-7.
8. Modic MT, Ross JS. Lumbar degenerative disk disease. *Radiology* 2007;245:43–61.
9. de Roos A, Kressel H, Spritzer C, et al. MR imaging of marrow changes adjacent to end plates in degenerative lumbar disk disease. *AJR Am J Roentgenol* 1987;149:531–4.
10. Modic MT, Steinberg PM, Ross JS, et al. Degenerative disk disease:

assessment of changes in vertebral body marrow with MR imaging. *Radiology* 1988;166:193–9.

11. Nerlich AG, Bachmeier BE, Schleicher E, et al. Immunomorphological analysis of RAGE receptor expression and NF-kappaB activation in tissue samples from normal and degenerated intervertebral discs of various ages. *Ann N Y Acad Sci* 2007;1096:239–48.
12. Poveda L, Hottiger M, Boos N, et al. Peroxynitrite induces gene expression in intervertebral disc cells. *SPINE* 2009;34:1127–33.
13. Sivan SS, Tsitron E, Wachtel E, et al. Age-related accumulation of pentosidine in aggrecan and collagen from normal and degenerate human intervertebral discs. *Biochem J* 2006;399:29–35.
14. Suzuki S, Fujita N, Hosogane N, et al. Excessive reactive oxygen species are therapeutic targets for intervertebral disc degeneration. *Arthritis Res Ther* 2015;17:316.
15. Chen K, Lv X, Li W, et al. Autophagy Is a Protective Response to the Oxidative Damage to Endplate Chondrocytes in Intervertebral Disc: Implications for the Treatment of Degenerative Lumbar Disc. *Oxid Med Cell Longev* 2017;2017:1–9.
16. Belge Kurutas E, Senoglu M, Yuksel KZ, et al. Oxidative/Nitrosative Stress in Patients With Modic Changes: Preliminary Controlled Study. *SPINE* 2015;40:1101–7.
17. Abderrazak A, Syrovets T, Couchie D, et al. Redox Biology NLRP3 in fl ammasome : From a danger signal sensor to a regulatory node of oxidative stress and in fl ammatory diseases. *Redox Biol* 2015;4:296–307.
18. Jones DP. Redefining Oxidative Stress. *Antioxid Redox Signal* 2006;8:1865–79.
19. Schroder K, Tschopp J. The Inflammasomes. *Cell* 2010;140:821–32.
20. Rathinam VA, Vanaja SK, Fitzgerald KA. Regulation of inflammasome signaling. *Nat Immunol* 2012;13:332–3.
21. Tschopp J, Schroder K. NLRP3 inflammasome activation: The convergence of

multiple signalling pathways on ROS production? *Nat Rev Immunol* 2010;10:210–5.

22. Tang P, Zhu R, Ji WP, et al. The NLRP3/Caspase-1/Interleukin-1β Axis Is Active in Human Lumbar Cartilaginous Endplate Degeneration. *Clin Orthop Relat Res* 2016;474:1818–26.
23. Martinon F, Burns K, Tschopp J rg. The Inflammasome: A Molecular Platform Triggering ctivation of Inflammatory Caspases and Processing of proIL-β. *Mol Cell* 2002;10:417–26.
24. Chen S, Huang Y, Zhou ZJ, et al. Upregulation of tumor necrosis factor alpha and ADAMTS-5, but not ADAMTS-4, in human intervertebral cartilage endplate with modic changes. *SPINE* 2014;39:E817-25.
25. Millward-Sadler SJ, Costello PW, Freemont AJ, et al. Regulation of catabolic gene expression in normal and degenerate human intervertebral disc cells: implications for the pathogenesis of intervertebral disc degeneration. *Arthritis Res Ther* 2009;11:R65.
26. Ajibade AA, Wang HY, Wang R. Cell type-specific function of TAK1 in innate immune signaling. *Trends Immunol* 2013;1–10.
27. Qiu ZX, Sha ZS, Che XM, et al. Correlation analysis of ADAMTS-4 , VCAM-1 , and TAK1 expression in cartilage tissue from spine tuberculosis Experimental group. *Genet Mol Res* 2017;16:1–8.
28. Shim J, Matthew B, Xie M, et al. TAK1 is an essential regulator of BMP signalling in cartilage. *EMBO J* 2009;28:2028–41.
29. Cheng J, Hu X, Dai L, et al. Inhibition of transforming growth factor β -activated kinase 1 prevents inflammation-related cartilage degradation in osteoarthritis. *Sci Rep* 2016;6:1–12.
30. Li CMD, Holz JDMS, Tang DMD, et al. IGF-1 regulation of type II collagen and MMP-13 expression in rat endplate chondrocytes via distinct signaling pathways. *Osteoarthr Cartil* 2009;17:100–6.
31. Han B, Zhu K, Li FC, et al. A Simple Disc Degeneration Model Induced by Percutaneous Needle Puncture in the Rat Tail. *SPINE* 2008;33:1925–34.

32. Zhang H, La Marca F, Hollister SJ, et al. Developing consistently reproducible intervertebral disc degeneration at rat caudal spine by using needle puncture. *J Neurosurg Spine* 2009;10:522–30.

33. Mao H, Chen Q, Han B, et al. The effect of injection volume on disc degeneration in a rat tail model. *SPINE* 2011;36:E1062-9.

34. Tang P, Gu J-M, Xie Z-A, et al. Honokiol alleviates the degeneration of intervertebral disc via suppressing the activation of TXNIP-NLRP3 inflammasome signal pathway. *Free Radic Biol Med* 2018;120:368–79.

35. Zhou Z, Tian F-M, Wang P, et al. Alendronate Prevents Intervertebral Disc Degeneration Adjacent to a Lumbar Fusion in Ovariectomized Rats. *SPINE* 2015;40:E1073–83.

36. Wang T, Zhang L, Huang C, et al. Relationship between osteopenia and lumbar intervertebral disc degeneration in ovariectomized rats. *Calcif Tissue Int* 2004;75:205–13.

37. Bauernfeind F, Bartok E, Rieger A, et al. Cutting Edge: Reactive Oxygen Species Inhibitors Block Priming, but Not Activation, of the NLRP3 Inflammasome. *J Immunol* 2011;187:613–7.

38. Zeng J, Chen Y, Ding R, et al. Isoliquiritigenin alleviates early brain injury after experimental intracerebral hemorrhage via suppressing ROS- and/or NF-?B-mediated NLRP3 inflammasome activation by promoting Nrf2 antioxidant pathway. *J Neuroinflammation* 2017;14:119.

39. Okada M, Matsuzawa A, Yoshimura A, et al. The Lysosome Rupture-activated TAK1-JNK Pathway Regulates NLRP3 Inflammasome Activation. *J Biol Chem* 2014;289:32926–36.

40. Dudli S, Fields AJ, Samartzis D, et al. Pathobiology of Modic changes. *Eur Spine J* 2016;25:3723–34.

41. Henrotin Y, Kurz B, Aigner T. Oxygen and reactive oxygen species in cartilage degradation: friends or foes? *Osteoarthr Cartil* 2005;13:643–54.

42. Abais JM, Xia M, Li G, et al. Contribution of endogenously produced reactive oxygen species to the activation of podocyte NLRP3 inflammasomes in

hyperhomocysteinemia. *Free Radic Biol Med* 2014;67:211–20.

43. Zhang L-L, Huang S, Ma X-X, et al. Angiotensin(1–7) attenuated Angiotensin II-induced hepatocyte EMT by inhibiting NOX-derived H 2 O 2 -activated NLRP3 inflammasome/IL-1β/Smad circuit. *Free Radic Biol Med* 2016;97:531–43.
44. Mihaly SR, Ninomiya-Tsuji J, Morioka S. TAK1 control of cell death. *Cell Death Differ* 2014;21:1667–76.
45. Fechtner S, Fox DA, Ahmed S. Transforming growth factor beta activated kinase 1: a potential therapeutic target for rheumatic diseases. *Rheumatol* 2017;56:1060-68.
46. Blaney Davidson EN, van Caam AP, Vitters EL, et al. TGF-beta is a potent inducer of Nerve Growth Factor in articular cartilage via the ALK5-Smad2/3 pathway. Potential role in OA related pain? *Osteoarthr Cartil* 2015;23:478–86.
47. Cheng J, Hu X, Dai L, et al. Inhibition of transforming growth factor beta-activated kinase 1 prevents inflammation-related cartilage degradation in osteoarthritis. *Sci Rep* 2016;6:34497.
48. Klatt AR, Klinger G, Neumuller O, et al. TAK1 downregulation reduces IL-1beta induced expression of MMP13, MMP1 and TNF-alpha. *Biomed Pharmacother* 2006;60:55–61.
49. Onodera Y, Teramura T, Takehara T, et al. Reactive oxygen species induce Cox-2 expression via TAK1 activation in synovial fibroblast cells. *FEBS Open Bio* 2015;5:492–501.
50. Xiao L, Saiki C, Okamura H. Oxidative Stress-Tolerant Stem Cells from Human Exfoliated Deciduous Teeth Decrease Hydrogen Peroxide-Induced Damage in Organotypic Brain Slice Cultures from Adult Mice. *Int J Mol Sci* 2019;20:E1858.
51. Heruye S, Maffofou N LN, Singh NU, et al. Standardization of a new method for assessing the development of cataract in cultured bovine lenses. *J Pharmacol Toxicol Methods* 2019;98:1–7.

Legends

Figure 1. Histological changes and altered extracellular matrices in cartilaginous endplates of patients with Modic changes. (A) Hematoxylin and eosin-stained (H&E) cartilaginous endplate specimens of the control group and the Modic changes group at ×100 magnification. Safranin O-stained cartilaginous endplate specimens at ×100. (B) The number of cartilaginous endplate cells from the control group and the Modic changes group. (C) Reactive oxygen species (ROS) levels in the cartilaginous endplate specimens. (D) Transcriptional levels of type II collagen (*Col II*), *SOX9*, matrix metalloproteinase (*MMP*)*13*, and *ADAMTS-5* are shown in cartilaginous endplate samples. (E) The protein expression levels of NLRP3, pro-caspase-1, caspase-1, pro-IL-1β, IL-1β, and transforming growth factor beta activated kinase 1 (TAK1) in cartilaginous endplates (CEP). (F) The concentration of mature IL-1β in endplate specimens. The data in the figures represent the mean ± S.D. Significant differences are indicated as *P < 0.05.

Figure 2. N-acetyl cysteine (NAC) treatment inhibits H_2O_2-induced rat endplate chondrocyte damage and oxidative stress. (A) Annexin V-FITC staining of endplate chondrocytes and the quantification of apoptosis. (B) Cell Counting Kit-8 (CCK-8) results of rat endplate chondrocytes treated with different concentrations of H_2O_2 for 24 h. (C) Malondialdehyde (MDA) content of chondrocytes treated with different concentrations of H_2O_2 for 24 h. (D) CCK-8 results of rat endplate chondrocytes

treated with different concentrations of NAC for 30 min. (E) Annexin V-FITC staining results of rat endplate chondrocytes pre-treated with NAC, MCC950, or diacerein and 1000 μM H_2O_2. (F) CCK-8 results of rat endplate chondrocytes pre-treated with NAC, MCC950, or diacerein and 1000 μM H_2O_2. (G) MDA content of chondrocytes pre-treated with NAC and then H_2O_2. (H) Activity of T-SOD in chondrocytes pre-treated with NAC and then H_2O_2. Data in the figures represent the mean ± S.D. Significant differences are indicated as *P < 0.05, **P < 0.01, ***P < 0.001, normal *vs* H_2O_2; $^{\#}$P < 0.05, $^{\#\#}$P < 0.01, $^{\#\#\#}$P < 0.001, H_2O_2 *vs* NAC, MCC950, or diacerein.

Figure 3. N-acetyl cysteine (NAC) inhibits H_2O_2-induced endplate chondrocyte extracellular matrix degradation. (A) Gene expression of extracellular matrix components in endplate chondrocytes. (B–F) Western blotting results of extracellular matrix components in endplate chondrocytes. Data in the figures represent mean ± S.D. Grey levels were normalized to β-actin. Significant differences are indicated as *P < 0.05, **P < 0.01.

Figure 4. Induction of signaling pathways by H_2O_2 in rat endplate chondrocytes. (A–D) Western blotting results of p-p65, p-JNK, and p-TAK1 in rat endplate chondrocytes treated with H_2O_2 for different time periods. The data in the figures represent the mean ± S.D. Grey levels were normalized to β -actin. Significant differences are indicated as *P < 0.05.

Figure 5. N-acetyl cysteine (NAC) and 5Z-7-O inhibit the activation of signaling pathways and the NLRP3 inflammasome. (A–G) Western blotting results of p-p65, p-JNK, p-TAK1, and the NLRP3/caspase-1/IL-1β axis in H_2O_2-induced rat endplate chondrocytes pre-treated with NAC or an inhibitor of TAK1 for 30 min. Data in the figures represent the mean ± S.D. Grey levels were normalized to β -actin. Significant differences are indicated as *P < 0.05, **P < 0.01.

Figure 6. A working model of lateral view of spinal column and illustrating that inhibiting reactive oxygen species (ROS) and TAK1 has protective effects against cartilaginous endplate (CEP) degeneration.

Figure 7. N-acetyl cysteine (NAC) and 5Z-7-O treatment ameliorate rat cartilaginous endplates (CEP) degeneration *in vivo*. (A) Representative Safranin O staining of disc samples from different experimental groups at 4 weeks post-surgery (original magnification ×4). (B) Representative Safranin O staining of CEPs from different experimental groups at 4 weeks post-surgery (original magnification ×40). (C) Representative H&E-stained CEPs from different experimental groups at 4 weeks post-surgery (original magnification ×40). (D) Representative CEP thickness of disc samples from different experimental groups at 4 weeks post-surgery. (E) The representative ratio of chondrocytes in CEPs from different experimental groups at 4 weeks post-surgery. Data in the figures represent the mean ± S.D. Significant differences are indicated as *P < 0.05, **P < 0.01, ***P < 0.001, control *vs* H_2O_2; $^{\#}$P < 0.05, $^{\#\#}$P < 0.01, $^{\#\#\#}$P < 0.001, NAC or 5Z-7-O *vs* H_2O_2.

Figure 8. Histological analysis of rat intervertebral disc degeneration (IVDD) at week 4 in different groups. (A) Representative H&E-stained nucleus pulposus (NP) from different experimental groups (original magnification ×40). (B) Representative H&E-stained annulus fibrosus (AF) from different experimental groups (original magnification ×40). (C) Expression of MMP13 in IVDs from different experimental groups. (D) Expression of IL-1β in IVDs from different experimental groups. (E) The histological scores of IVDs from different experimental groups. (F) Integrated optical densities of MMP-13 in IVDs. (G) Percentage of cells positive for IL-1β in IVDs. (H) Representative IVD revealed by MRI based on T2-weighted images. (I) Quantitative analysis of T2 disc signal intensity. Data in the figures represent the mean ± S.D. Significant differences are indicated as *P < 0.05, **P < 0.01, control *vs* H_2O_2; $^{\#}$P < 0.05, $^{\#\#}$P < 0.01, NAC or 5Z-7-O *vs* H_2O_2.

Table 1. Primer sequences used for quantitative RT-PCR.

Gene	Species	Direction	Sequences 5`-3`
Col II	Human	Forward	CTGGAAAAGCTGGTGAAAGG
		Reverse	GGCCTGGATAACCTCTGTGA
SOX-9	Human	Forward	GGAATGTTTCAGCAGCCAAT
		Reverse	TGGTGTTCTGAGAGGCACAG
MMP13	Human	Forward	TGGTCCAGGAGATGAAGACC
		Reverse	TCCTCGGAGACTGGTAATGG
ADAMTS-5	Human	Forward	TACTTGGCCTCTCCCATGAC
		Reverse	TTTGGACCAGGGCTTAGATG
β-actin	Human	Forward	AGCGAGCATCCCCCAAAGTT
		Reverse	GGGCACGAAGGCTCATCATT
Col II	Rat	Forward	AAGGGACACCGAGGTTTCACTGG
		Reverse	GGGCCTGTTTCTCCTGAGCGT
SOX-9	Rat	Forward	AGCGACAACTTTACCAG
		Reverse	GGAAAACAGAGAACGAAAC
MMP13	Rat	Forward	TGCTGCATACGAGCATCCAT
		Reverse	TTCCCCGTGTCCTCAAAGTG
ADAMTS-5	Rat	Forward	GTCCAAATGCACTTCAGCCACGAT
		Reverse	AATGTCAAGTTGCACTGCTGGGTG
NLRP3	Rat	Forward	CGGTGACCTTGTGTGTGCTT
		Reverse	TCATGTCCTGAGCCATGGAAG
Caspase-1	Rat	Forward	GAACAAAGAAGGTGGCGCAT
		Reverse	AGACGTGTACGAGTGGGTGT
IL-1β	Rat	Forward	CCTATGTCTTGCCCGTGGAG
		Reverse	CACACACTAGCAGGTCGTCA
β-actin	Rat	Forward	TTGTAACCAACTGGGACGATATGG
		Reverse	GATCTTGATCTTCATGGTGCTAGG

Abbreviations:
RT-PCR = Reverse Transcription Polymerase Chain Reaction;
Col II = Type II collagen;
MMP3 = matrix metalloproteases, 3;
ADAMTS-5 = a disintegrin-like and metalloprotease with thrombospondin type I motifs-5;
NLRP3 = NACHT, LRR and PYD domains-containing protein, 3;

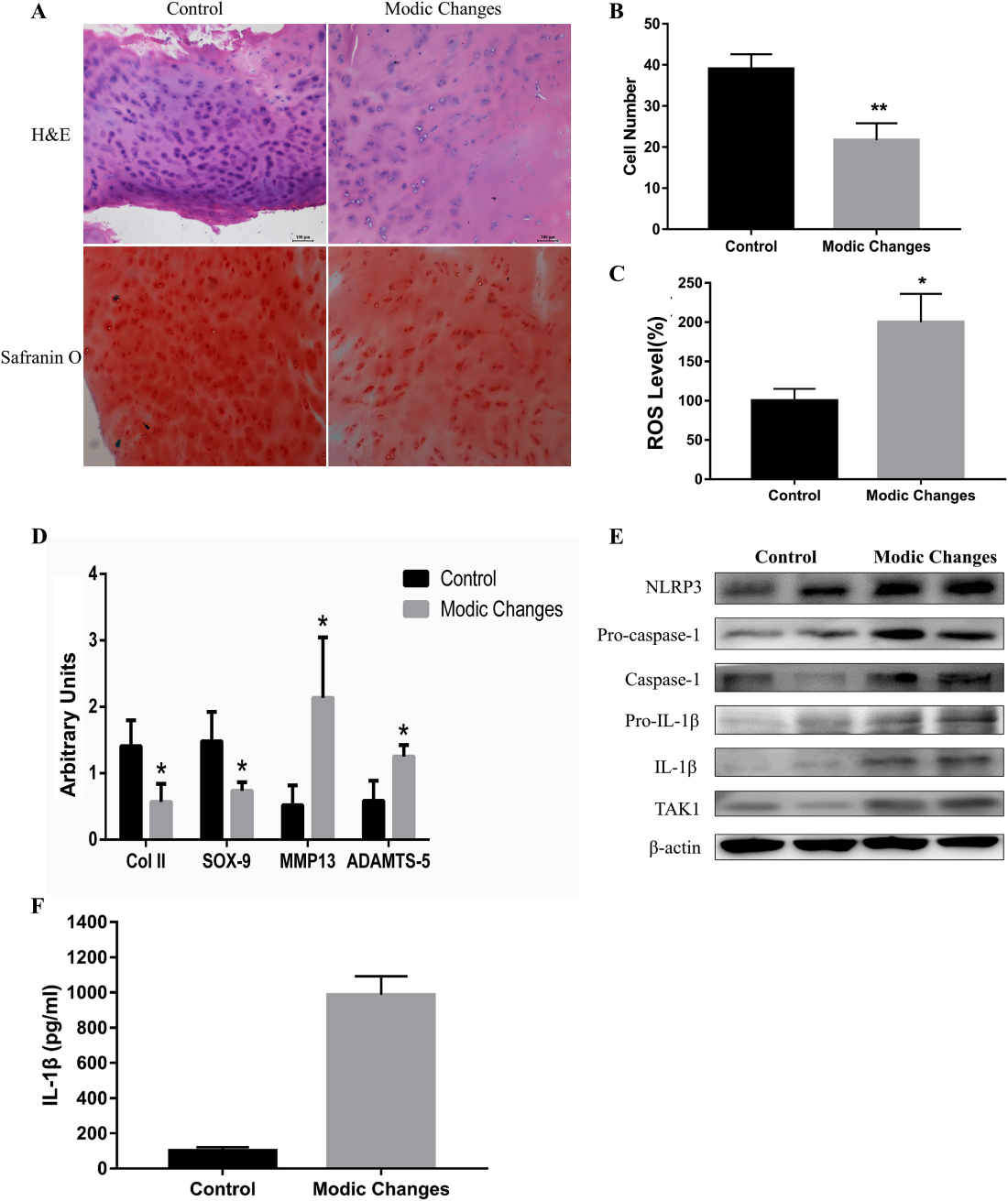
A
Control
Modic Changes
H&E
Safranin O
B
Cell Number
50
40
30
20
10
0
**
Control
Modic Changes
C
ROS Level(%)
250
200
150
100
50
0
*
Control
Modic Changes
D
Arbitrary Units
4
3
2
1
0
Control
Modic Changes
*
Col II
SOX-9
MMP13
ADAMTS-5
E
Control
Modic Changes
NLRP3
Pro-caspase-1
Caspase-1
Pro-IL-1β
IL-1β
TAK1
β-actin
F
IL-1β (pg/ml)
1400
1200
1000
800
600
400
200
0
Control
Modic Changes

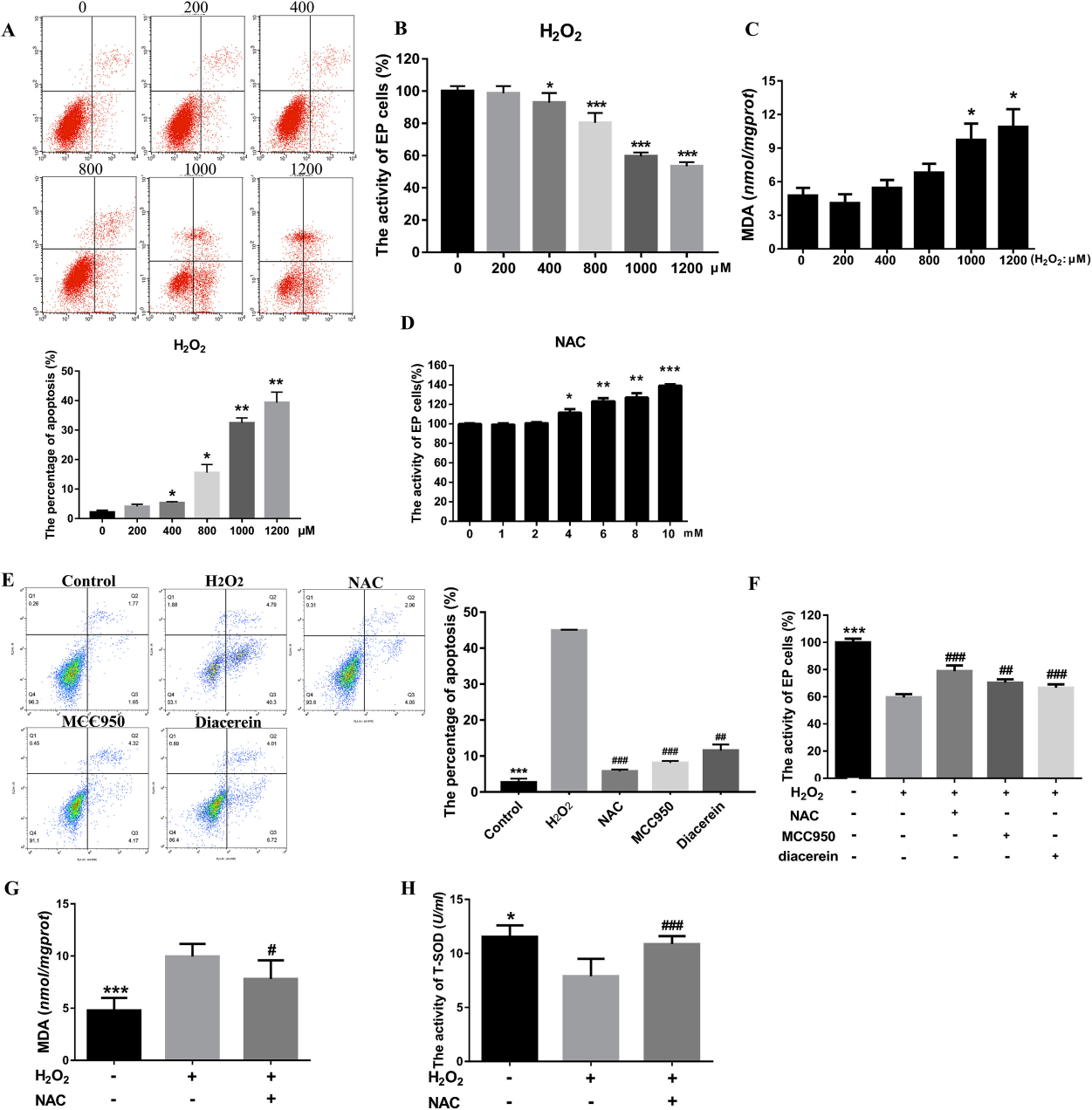
A
0
200
400
800
1000
1200
B
H2O2
The activity of EP cells (%)
0 200 400 800 1000 1200 μM
C
MDA (nmol/mgprot)
0 200 400 800 1000 1200 (H2O2: μM)
H2O2
The percentage of apoptosis (%)
0 200 400 800 1000 1200 μM
D
NAC
The activity of EP cells(%)
0 1 2 4 6 8 10 mM
E
Control
H2O2
NAC
MCC950
Diacerein
The percentage of apoptosis (%)
Control
H2O2
NAC
MCC950
Diacerein
F
The activity of EP cells (%)
H2O2
NAC
MCC950
diacerein
G
MDA (nmol/mgprot)
H2O2
NAC
H
The activity of T-SOD (U/ml)
H2O2
NAC

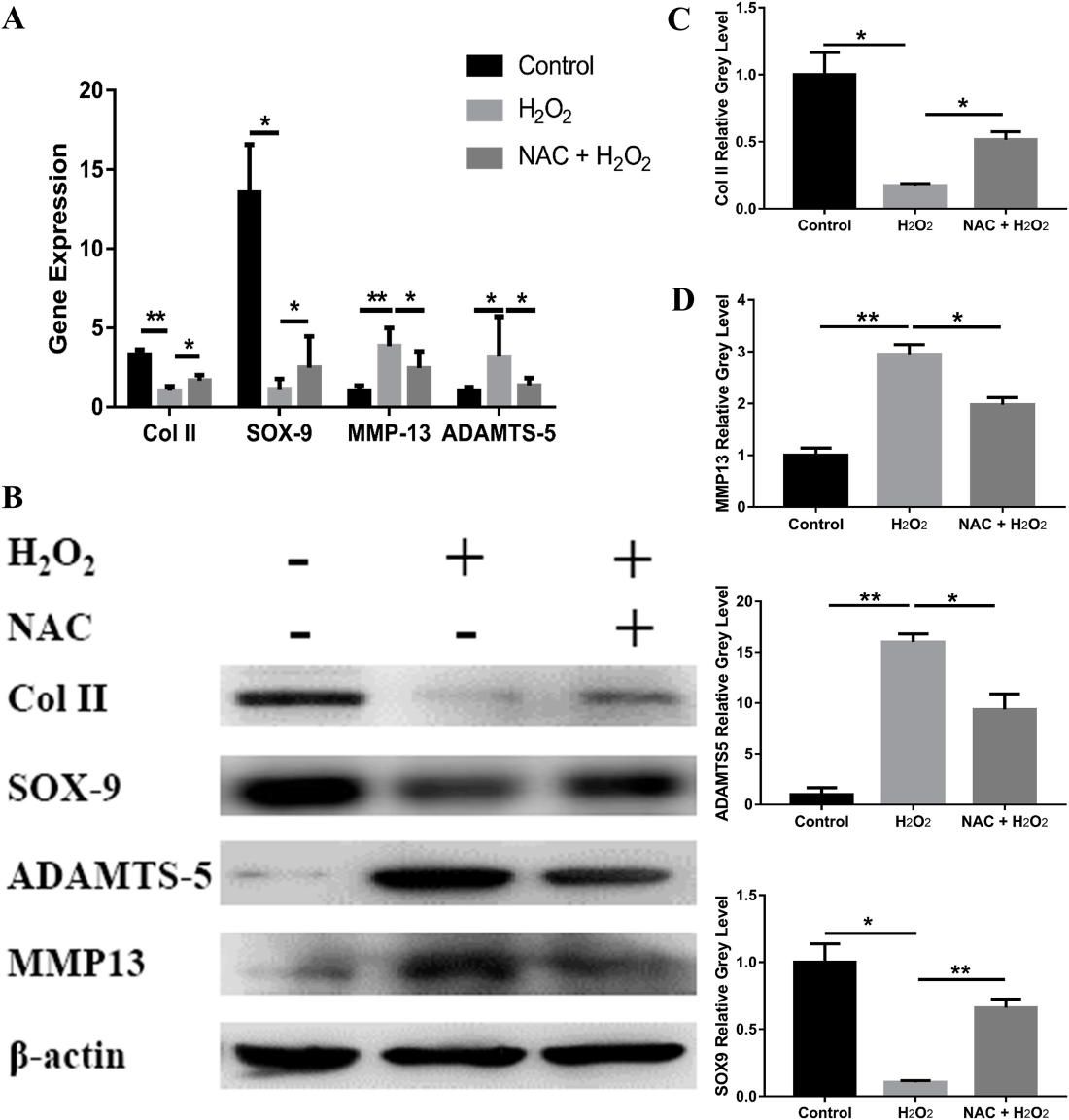
A
Control
H2O2
NAC + H2O2
Gene Expression
20
15
10
5
0
Col II
SOX-9
MMP-13
ADAMTS-5
B
H2O2
NAC
Col II
SOX-9
ADAMTS-5
MMP13
β-actin
C
Col II Relative Grey Level
1.5
1.0
0.5
0.0
Control
H2O2
NAC + H2O2
D
MMP13 Relative Grey Level
4
3
2
1
0
ADAMTS5 Relative Grey Level
20
15
10
5
0
SOX9 Relative Grey Level
1.5
1.0
0.5
0.0

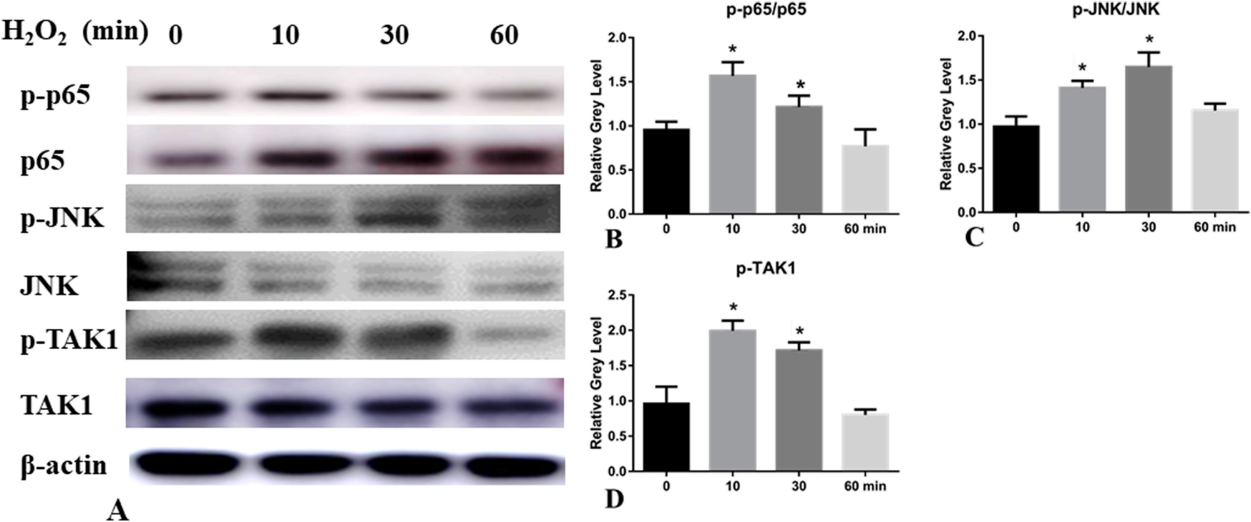
H2O2 (min) 0 10 30 60
p-p65
p65
p-JNK
JNK
p-TAK1
TAK1
β-actin
A
p-p65/p65
Relative Grey Level
2.0
1.5
1.0
0.5
0.0
0 10 30 60 min
B
p-JNK/JNK
Relative Grey Level
2.0
1.5
1.0
0.5
0.0
0 10 30 60 min
C
p-TAK1
Relative Grey Level
2.5
2.0
1.5
1.0
0.5
0.0
0 10 30 60 min
D

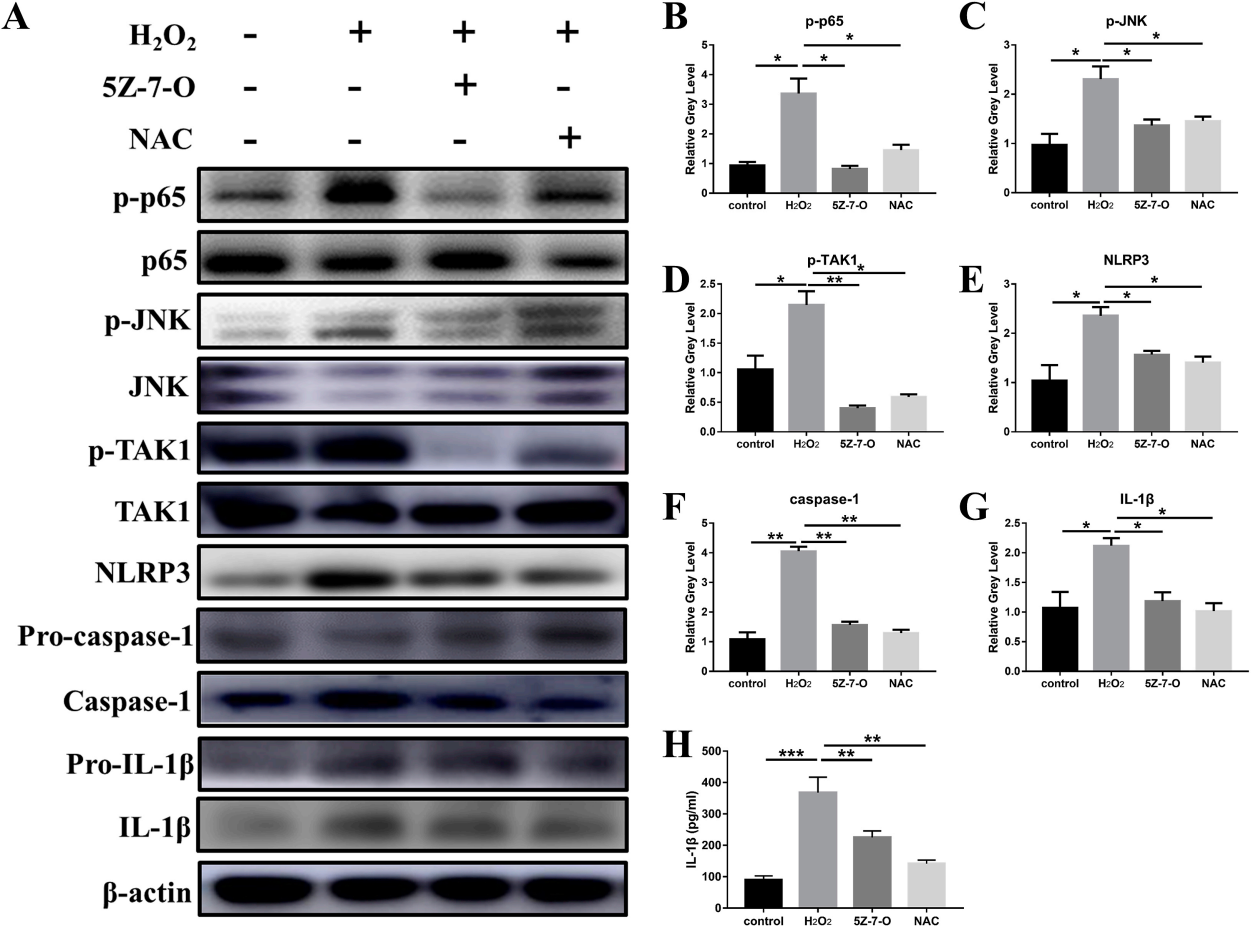
A
H2O2 - + + +
5Z-7-O - - + -
NAC - - - +
p-p65
p65
p-JNK
JNK
p-TAK1
TAK1
NLRP3
Pro-caspase-1
Caspase-1
Pro-IL-1β
IL-1β
β-actin
B
p-p65
C
p-JNK
D
p-TAK1
E
NLRP3
F
caspase-1
G
IL-1β
H
IL-1β (pg/ml)
Relative Grey Level
control
H2O2
5Z-7-O
NAC

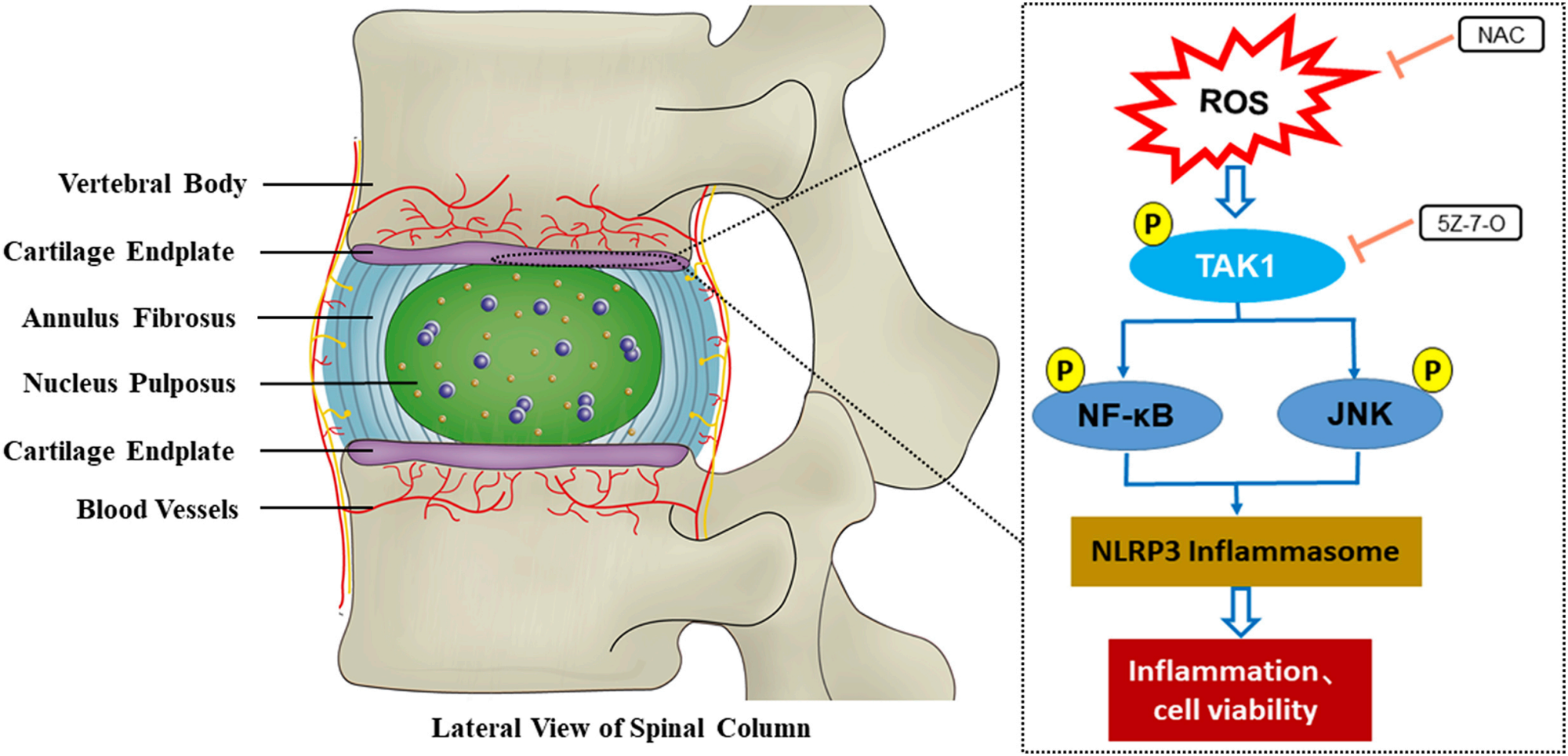
Vertebral Body
Cartilage Endplate
Annulus Fibrosus
Nucleus Pulposus
Cartilage Endplate
Blood Vessels
Lateral View of Spinal Column
ROS
NAC
P
TAK1
5Z-7-O
P
NF-κB
P
JNK
NLRP3 Inflammasome
Inflammation、
cell viability

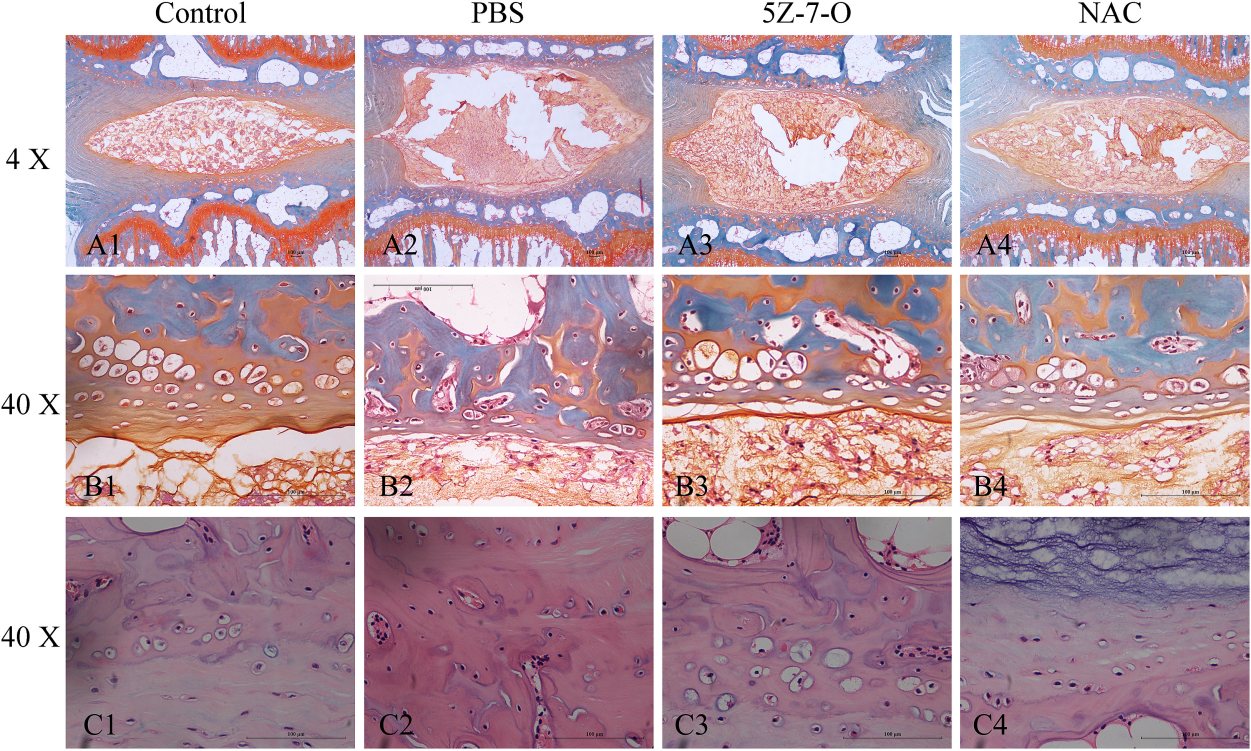
Control
PBS
5Z-7-O
NAC
4 X
40 X
40 X
A1
A2
A3
A4
B1
B2
B3
B4
C1
C2
C3
C4

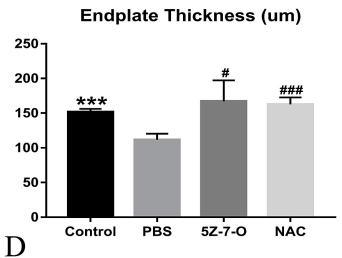
Endplate Thickness (um)
250
200
150
100
50
0
***
#
###
Control
PBS
5Z-7-O
NAC

D

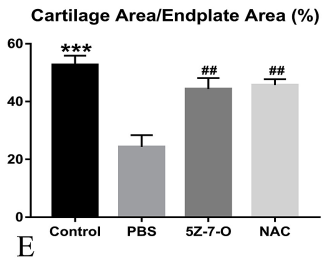
Cartilage Area/Endplate Area (%)
60
40
20
0
***
##
##
Control
PBS
5Z-7-O
NAC

E

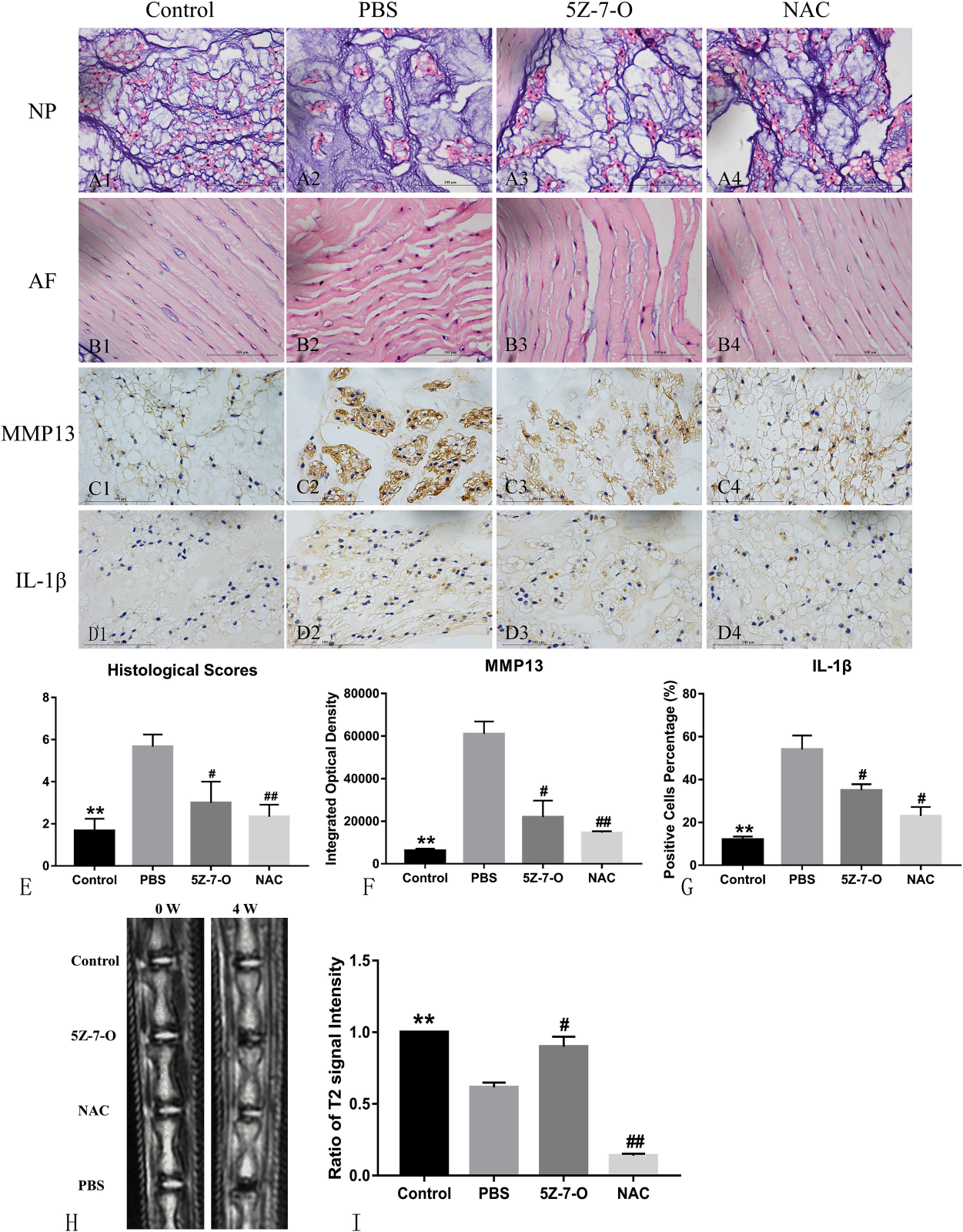
Control
PBS
5Z-7-O
NAC
NP
AF
MMP13
IL-1β
A1
A2
A3
A4
B1
B2
B3
B4
C1
C2
C3
C4
D1
D2
D3
D4
Histological Scores
MMP13
IL-1β
Integrated Optical Density
Positive Cells Percentage (%)
Control
PBS
5Z-7-O
NAC
E
F
G
0 W
4 W
Control
5Z-7-O
NAC
PBS
H
Ratio of T2 signal Intensity
I

Highlights

An H_2O_2 induced oxidative stress model of the endplate was successfully established *in vitro* as well as *in vivo.*

NAC alleviated cellular damage, abrogated catabolic effects and restored the redox status and cell viability in endplate chondrocytes *in vitro* and *in vivo*.

The small molecule inhibitor of transforming growth factor b-activated kinase-1 (TAK1), 5Z-7-O, reduced the expression of p-TAK1 and NLRP3 considerably, and ameliorated rat CEP degeneration *in vivo.*